Mechanical Regulation of the Magnetic Properties of Uniaxial Anisotropic Hexaferrite Thin Films

Qishan Zhu,[1] Rujun Tang,[1,*] Feng Peng,[1] Sichen Xu,[1] Guoqing Liang,[1] Run Zhao,[2] Yong Fang,[3] Lu You,[1] and Xiaodong Su[1]

[1] *Jiangsu Key Laboratory of Thin Films, School of Physical Science and Technology, Soochow University, Suzhou 215006, People's Republic of China*

[2] *School of Physical Science and Technology, Suzhou University of Science and Technology, Suzhou 215003, People's Republic of China*

[3] *Jiangsu Laboratory of Advanced Functional Materials, Department of Physics, Changshu Institute of Technology, Changshu 215500, People's Republic of China*

(Received 15 June 2021; revised 1 September 2021; accepted 20 October 2021; published 2 November 2021)

Flexible oxide thin films with uniaxial magnetocrystalline anisotropy (K_u) not only have many applications in flexible electronics, but also provide an ideal low-crystal-symmetry material for a fundamental understanding of the competitive interplay among magnetocrystalline anisotropy, shape anisotropy, and stress anisotropy. However, an understanding of the mechanical tuning of magnetic parameters in flexible oxide films with K_u has not been realized up to now. In this work, epitaxial flexible hexaferrite $BaFe_{12}O_{19}$ thin films with a room temperature out-of-plane K_u of 1.1×10^5 J/m^3 are fabricated. The continuous and controllable tuning of magnetic parameters is found to be realizable by different bending radii of the film. The changes in magnetic parameters are symmetrical under tensile and compressive bending due to the dominance of film geometry and bending-stress directions, which are perpendicular to the easy axis of K_u. The micromagnetic simulations further show that the magnitude of K_u plays a critical role in the mechanical tuning performance of the film, where high K_u drastically reduces the role of stress anisotropy and increases the magnetic bending repeatability of the film by suppressing bending-defect-related anisotropy degradation. This work not only provides an understanding of the role of the direction and magnitude of K_u in the flexible thin films, but also demonstrates that the flexible hexaferrite film is one of the best materials for mechanical tunable devices up to the millimeter-wave region.

DOI: 10.1103/PhysRevApplied.16.054006

I. INTRODUCTION

Magnetic materials with high uniaxial magnetocrystalline anisotropy (K_u) are critical to realizing some functional devices, including perpendicular magnetic recording media, magnetic random access memory, permanent magnets, and microwave devices [1–4]. Although many metal magnetic alloys and ultrathin films with high K_u have been discovered, magnetic oxides with high K_u are still rare in nature, especially those with room-temperature K_u [3–7]. This should be due to the physical difficulty of the coexistence of large magnetization, strong spin-orbit interaction, and low crystal symmetry in oxides [5]. Moreover, with the miniaturization of communication electronics, the next generation (fifth generation and above) of microwave-transceiver components boosts the demands for magnetic oxide thin or thick films with high K_u and *in situ* tunability [4,8–10]. The *in situ* tuning of magnetic anisotropy can be achieved by either electric fields (inversed magnetoelectric effect) or mechanical strain [11–13]. In multiferroic devices, the magnetoelectric effect is also realized through the use of strain- and stress-mediated interactions [14]. Compared with electric tunable multiferroic devices, purely mechanical strain- and stress- (without electric driven) tunable epitaxial thin films have many advantages: (i) free of an electric field, (ii) it is not necessary to consider the complex interface properties between magnetic and ferroelectric phases, and (iii) it is not necessary to think of the mode of magnetoelectric coupling and the orientation of electric fields [15]. Based on the above advantages, purely mechanical strain-tunable anisotropy is suitable for some noncontact passive systems and flexible devices.

For magnetic thin films under mechanical loading, an understanding of the competitive interplay among magnetocrystalline anisotropy, shape anisotropy, and stress anisotropy will be critical for device applications. The mechanical tuning of anisotropy in soft magnetic metal thin films is widely investigated [10]. Stress anisotropy is

*tangrj@suda.edu.cn

found to play a central role in those soft magnetic thin films. However, the soft magnetic nature of the above metal thin films restricts their applications in ultrahigh-frequency devices. For this reason, some flexible spinel-ferrite thin films, such as $Y_3Fe_5O_{12}$, Fe_3O_4, $CoFe_2O_4$, $CuFe_2O_4$, and $LiFe_5O_8$, have also been reported to investigate their fabrication compatibility and stress-tunable magnetic properties [16–22]. A flexible thin film with K_u not only has many applications in flexible devices, but also provides an ideal low-crystal-symmetry material for understanding the competitive interplays among magnetic anisotropies in thin films. However, the cubic structure of spinel ferrites makes K_u symmetrically inaccessible [16–22]. An understanding of the mechanical tuning of K_u in flexible oxide films has not been realized up to now.

Here, we choose the M-type hexaferrite $BaFe_{12}O_{19}$ (hereafter referred to as BaM) as a model material due to its hexagonal crystal structure ($P6_3/mmc$), which permits a high room-temperature K_u [4,23]. With the merits of high K_u and moderate M_s, BaM is used in permanent magnets, magnetic recording media, and microwave devices with a ferromagnetic resonance frequency above 40 GHz [23–25]. In addition, the hexagonal crystal structure of BaM enables potential epitaxy on single-crystalline substrates like sapphire [26–29]. However, a flexible single-crystalline BaM thin film has never been fabricated. To get a high-K_u flexible BaM thin film, in this study, the integration of BaM thin films on single-crystalline mica substrate is first investigated. Then, epitaxial BaM thin films are made flexible by substrate thinning. Finally, the magnetic properties, mechanical tunability, and bending stability of flexible BaM films are investigated both experimentally and theoretically.

II. SAMPLES AND METHODS

A. Sample fabrication

The epitaxial BaM thin films (10×20 mm^2) are first prepared on single-crystalline fluorophlogopite (mica) substrate by pulsed laser deposition (PLD, Lambda Physik, 248 nm, 8 Hz, 0.45 J/cm^2) using a $BaFe_{12}O_{19}$ ceramic target. The base vacuum pressure in the PLD chamber is 2×10^{-4} Pa. Thin-film growth takes place at 790 °C in 15 Pa flowing O_2 gas. After the growth of films is completed, the films are *in situ* annealed at 790 °C for 10 min under an O_2 atmosphere at a pressure of 1×10^4 Pa to increase their crystallinity, and then cooled down to room temperature under the same atmosphere. Flexible BaM films are obtained by mechanical peeling from the back of the mica substrate [30].

B. Microstructure and magnetic characterizations

The crystal structures and epitaxial nature of the BaM/mica films are characterized by x-ray diffraction (XRD, Rigaku DMax 2000 PC), Raman spectroscopy (Horiba Xplore), and transmission electron microscopy (TEM, Tecnai FEI G^2 F20) at room temperature. The surface morphology of the films is characterized by scanning electron microscopy (SEM, FEI). The magnetic properties of the samples are measured with a vibrating sample magnetometer and torque magnetometer in a physical property measurement system (PPMS-9, Quantum Design). For bending-radius-dependent magnetic property measurements, the BaM film is cut down to 2×4 mm^2 and attached onto rigid polyethylene terephthalate surfaces with different curvatures. The bending cycles are realized by a fixture driven by a stepping motor.

C. Micromagnetic simulations

Micromagnetic simulation of the flexible BaM thin film is made with the OOMMF2.a2 software by solving the Landau-Lifshitz-Gilbert equation [30,31]. The average energy density, E, includes magnetic anisotropy, exchange, demagnetization, and Zeeman terms. The anisotropy term in this work includes two parts: the magnetocrystalline anisotropy and the bending-stress anisotropy. Simulation of the bent BaM film is realized with different curved cuboids with a constant arc length of 1000 nm, width of 500 nm, and thickness of 50 nm. The arc radius, R, varies from ∞ to 1.5 mm. The BaM films are then discretized with a cell size of $5 \times 5 \times 5$ nm^3 in three-dimensional space. The material parameters used in the simulations are our experimental values of the BaM film with saturation magnetization $M_s = 1.51 \times 10^5$ A/m and $K_u = 1.1 \times 10^5$ J/m^3. The exchange constant, $A = 6.3 \times 10^{-12}$ J/m, is taken from Ref. [32]. The Gilbert damping parameter is set to 0.2. To get a better comparison with experimental results, the crystalline c axis of all BaM films is set to be six degrees of random distribution away from the film normal directions, $\vec{n}$. The external magnetic fields (-20 kOe $\leq H \leq 20$ kOe) are applied along the out-of-plane, in-plane, and crossover directions. Finally, the magnetization-reversal processes of the BaM films with different bending radii, strain directions, and density of cracks are simulated.

III. RESULTS AND DISCUSSION

A. Microstructure and magnetic characterizations of flat BaM films on mica

Figure 1 shows the microstructures of the BaM film grown on mica substrate. Figure 1(a) shows that only BaM (00n) peaks are observed for the BaM film grown on mica (001) substrate, almost identical to that of the BaM film on a sapphire substrate, which is the most widely used substrate for BaM epitaxy [29]. Figure 1(b) shows reciprocal space mapping around the BaM (006)/mica (003) and BaM (008)/mica (003) reflections. It is clear that the BaM film

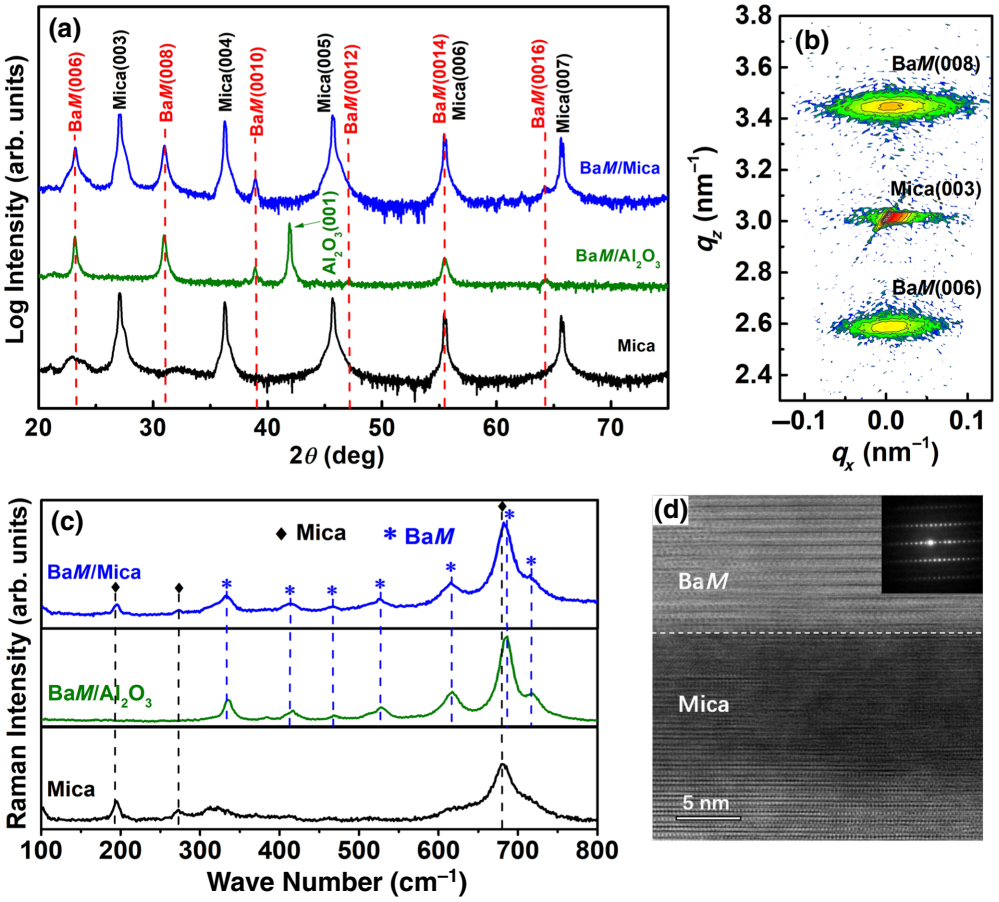

FIG. 1. (a) XRD patterns of Ba*M* films grown on mica and sapphire substrates. (b) XRD mapping of mica (003), Ba*M* (006), and Ba*M* (008) peaks of the film grown on mica substrate. (c) Raman spectra of Ba*M* films on mica and sapphire substrates. (d) TEM cross-section image and selected-area diffraction pattern of the Ba*M*/mica sample.

possesses well-defined diffraction peaks, indicating good crystallinity and the epitaxial nature of Ba*M*. The Raman spectrum in Fig. 1(c) also shows the same peaks of Ba*M* on mica as those on sapphire, implying identical crystal structures. The TEM cross-section image in Fig. 1(d) further shows that the film-substrate interface is sharp.

Figure 2(b) shows the hysteresis loops of the Ba*M* film (thickness of 180 nm) grown on mica (001) substrate. The flexible Ba*M* film has a small in-plane coercivity of 165 Oe and a large H_c out-of-plane coercivity of 2401 Oe, showing a large uniaxial magnetic anisotropy along the out-of-plane direction.

Ba*M* films with different thicknesses all show uniaxial magnetic anisotropy [30]. To obtain the magnetic anisotropy constants of the Ba*M* film, the magnetic torque curve is measured, as shown in Fig. 2(c). According to the symmetry of the hexagonal structure, the field-angle-(θ) dependent magnetic torque (T) can be defined with the following equation by neglecting high-order terms [33]:

$$T(\theta) = -\frac{\partial E_{K_u}}{\partial \theta} = -(K_{u1} + K_{u2})\sin 2\theta + \frac{K_{u2}}{2}\sin 4\theta, \tag{1}$$

where E_{K_u} is the magnetic anisotropic energy; the easy direction corresponds to the orientation for which E_{K_u} is minimal. The first- and second-order uniaxial anisotropies, K_{u1} and K_{u2}, can have uniaxial anisotropy. Then, the total anisotropy of the Ba*M* film, K_u , can be obtained by [33]

$$K_u = K_{u1} + K_{u2} + \frac{1}{2}\mu_0 M_s^2, \tag{2}$$

where the M_s value obtained is 151 emu/cm^3; K_u for the Ba*M* film in Figs. 2(b) and 2(c) is calculated to be 1.1×10^5 J/m^3. This high H_K supports an out-of-plane zero-field ferromagnetic resonance frequency, f_r, of about 37 GHz from [4,26]

$$f_r = \gamma(H_K - 4\pi M_s), \tag{3}$$

where $\gamma = 2.8$ MHz/Oe. Moreover, the high K_u brings about large differences between the out-of-plane and in-plane magnetic components, with the simultaneous appearance of a large coercivity ratio, $H_{c\text{-out}}/H_{c\text{-in}}$, and remanence ratio, $M_{r\text{-out}}/M_{r\text{-in}}$. Figure 2(d) shows that large ratios of $H_{c\text{-out}}/H_{c\text{-in}}$ and $M_{r\text{-out}}/M_{r\text{-in}}$ exist for Ba*M* films with different thicknesses, despite the coercivity and remanence of Ba*M* films varying with thickness. Superhigh $H_{c\text{-out}}/H_{c\text{-in}}$ and $M_{r\text{-out}}/M_{r\text{-in}}$ are observed simultaneously when the film thickness exceeds 180 nm. To benchmark the anisotropic

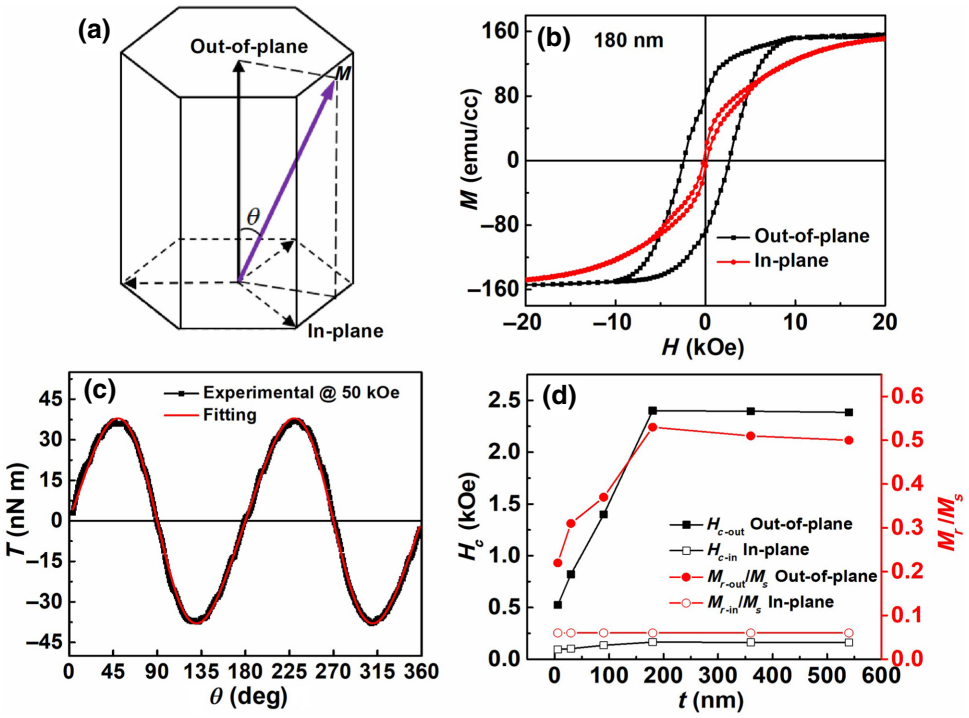

FIG. 2. (a) Schematics of crystal symmetry of BaM film with magnetization, M, deviating by angle θ from the out-of-plane direction. (b) Out-of-plane and in-plane hysteresis loops of flat BaM film (thickness 180 nm) on mica (001) substrate. (c) Angular magnetic torque (T) of flat BaM film under magnetic field of 50 kOe. (d) Thickness- (t) dependent coercivity, H_c, and remanence ratios, M_r/M_s, of flexible BaM films.

magnetism of the flexible BaM film, the magnetic properties of all reported flexible ferrite thin films are summarized in Table I. The simultaneous presence of the high $H_{c\text{-out}}/H_{c\text{-in}}$ and $M_{r\text{-out}}/M_{r\text{-in}}$ indicates a high K_u. For this reason, we compare $H_{c\text{-out}}/H_{c\text{-in}}$ and $M_{r\text{-out}}/M_{r\text{-in}}$ of various flexible ferrite films because their K_u values are not available in Refs. [16–22]. It can be seen that, among available flexible ferrite films, only BaM has uniaxial magnetic anisotropy with $M_{r\text{-out}}/M_{r\text{-in}}$ up to 7.95. Moreover, $H_{c\text{-out}}/H_{c\text{-in}}$ of the BaM film with a thickness of 180 nm reaches 14.55, in good agreement with the superhigh K_u of the flexible BaM film. Magnetic thin films in flexible devices in action will be subject to different bending conditions. Hence, the magnetic properties of the BaM films under different bending radii and bending cycles are studied. The bending strain, ε_b, in the bent BaM films can be approximately calculated by [20,21]

$$\varepsilon_b = \frac{t_s + t_f}{2R} \frac{(1 + 2\eta + \chi\eta^2)}{(1+\eta)(1+\chi\eta)}, \tag{4}$$

where t_s and t_f are the thicknesses of the substrate and film, respectively. $\eta = t_f/t_s$ and $\chi = E_f/E_s$; E_s and E_f are the Young's modulus of the substrate and film, respectively. In this work, E_s and E_f are 5.4×10^{10} and 1.35×10^{12} dynes/cm^2, respectively [34]. If $t_s = 12$ μm and $t_f = 180$ nm, for bending radii of $R = 5.5$, 3.5, and 1.5 mm, the ε_b values calculated with Eq. (3) are $\varepsilon_b = 0.3\%$, 0.6%, and 1.3%, respectively. The SEM images show that the BaM film remains intact, even at the largest bending radius

TABLE I. Comparison of magnetic parameters between the flexible BaM film (thickness: 180 nm) and other reported flexible ferrite films in the flat state; M_s is the saturation magnetization, $H_{c\text{-out}}$, $H_{c\text{-in}}$, $M_{r\text{-out}}$, and $M_{r\text{-in}}$ are the out-of-plane and in-plane coercivity and remanence, respectively. The coercivity and remanence ratios, $H_{c\text{-out}}/H_{c\text{-in}}$ and $M_{r\text{-out}}/M_{r\text{-in}}$, are provided for comparison because their K_u values are not available in the literature.

Flexible materials	Film state	M_s (emu/cm^3)	$H_{c\text{-out}}$ (Oe)	$H_{c\text{-in}}$ (Oe)	$H_{c\text{-out}}/H_{c\text{-in}}$	$M_{r\text{-out}}/M_{r\text{-in}}$
$BaFe_{12}O_{19}$	Epitaxial	151	2401	165	14.55	7.95
Fe_3O_4 [16]	Epitaxial	580	502	182	2.76	0.38
$CoFe_2O_4$ [19]	Epitaxial	115	1020	1222	0.83	1.44
$LiFe_5O_8$ [20]	Epitaxial	155	113	159	0.71	1.05
$CuFe_2O_4$ [21]	Epitaxial	140	165	165	1	0.17
$Y_3Fe_3O_{12}$ [22]	Polycrystalline	139	123	20	6.15	0.3

of 1.5 mm [30]. Although bulk oxides are brittle, excellent mechanical flexibility can be realized at the nanoscale, as observed in $BaTiO_3$ and Fe_3O_4 thin films [17,18,35,36].

B. Bending-curvature-dependent magnetic properties of Ba*M* thin films

Figure 3 provides a comparison of the magnetic hysteresis loops of Ba*M* films under different bending radii and strains (both tensile and compressive). The magnetic fields are applied in in-plane, crossover, and out-of-plane directions to the film surface. Figures 3(b)–3(d) show that, when the magnetic field is applied along the in-plane direction, the hysteresis loops are almost unchanged under both tensile and compressive bending. This suggests that the bending curvature and bending strains do not lead to notable changes to the in-plane magnetization-reversal process of the Ba*M* film. This further confirms that the Ba*M* films grow well with strong out-of-plane K_u. When the magnetic field is applied from the crossover and out-of-plane directions, the hysteresis loops change slightly. However, the change in the hysteresis loop is small when R is larger than 3.5 mm. Notable changes are observed when R is reduced to 1.5 mm. Moreover, tensile bending and compressive bending also lead to some differences in the hysteresis loops.

To better analyze the curvature-dependent magnetic properties of the Ba*M* film, we define an effective anisotropy constant, $K_{u\text{eff}}$, including contributions from uniaxial magnetocrystalline anisotropy (K_u), stress anisotropy, and shape anisotropy (geometry of the film). The bending-curvature-dependent coercivity, H_c; remanence ratios, M_r/M_s; and $K_{u\text{eff}}$ are summarized in Figs. 3(e)–3(g). The curvature-dependent $K_{u\text{eff}}$ is deduced from the area difference of demagnetization curves between in-plane and out-of-plane hysteresis loops due to the mass limitation (<10 mg) of the torque method for a fixed bent film [37]. $K_{u\text{eff}}$ of flat Ba*M* on mica calculated by the area-difference method is 1.01×10^5 J/m^3, which is slightly smaller than that in Fig. 2. Figures 3(e) and 3(f) show that, when the magnetic field is applied along the in-plane direction, both H_c and M_r are almost identical until $R = 1.5$ mm, suggesting an undisturbed magnetization-reversal process of the Ba*M* film along the in-plane direction during bending. When the magnetic field is applied from the crossover and out-of-plane directions,

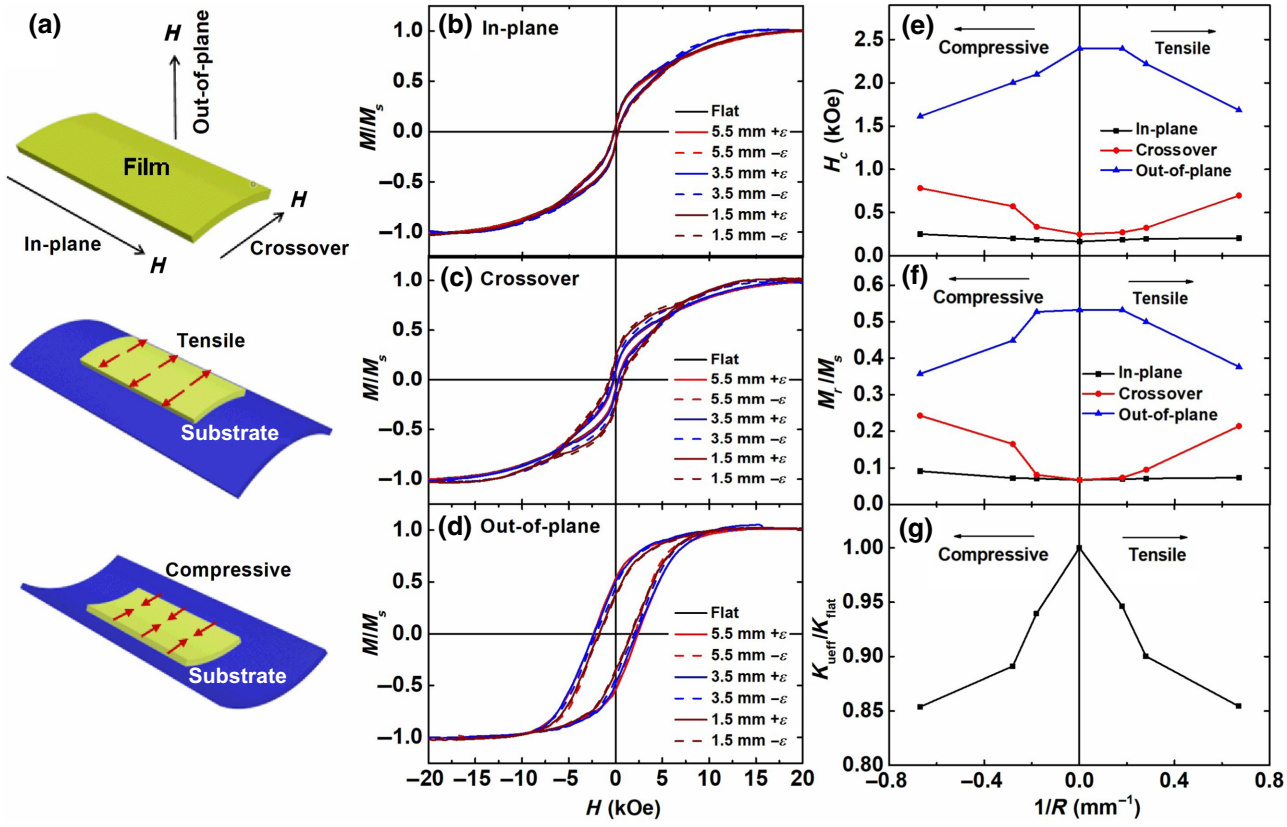

FIG. 3. (a) Schematic illustrations of testing methods for bent film; (b)–(d) magnetic hysteresis loops (in-plane, crossover, and out-of-plane) of flexible Ba*M* film (thickness 180 nm) under different bending radii, R, of $R = \infty$ (flat), 5.5, 3.5, and 1.5 mm. Tensile ($+\varepsilon$) and compressive ($-\varepsilon$) strains are indicated; (e)–(g) bending-curvature-dependent coercivity, H_c; remanence ratios, M_r/M_s; and $K_{u\text{eff}}$, respectively; $K_{\text{flat}} = 1.01 \times 10^5$ J/m^3.

notable changes to H_c and M_r/M_s are observed when R is smaller than 5.5 mm. Each decrease in the out-of-plane H_c (M_r/M_s) leads to an increase in the crossover H_c (M_r/M_s) of almost the same magnitude. This leads to an almost symmetrical decrease of $K_{u\text{eff}}$ under tensile and compressive strains, as shown in Fig. 3(g). The above results indicate that changes to the magnetization-reversal process of BaM films are dominated by their film geometries (shape anisotropy). The deviation of the crystalline c axis from the applied-field direction in a curved film will lead to a symmetrical reduction of magnetic parameters ($H_{c\text{-out}}$, $M_{r\text{-out}}$, and $K_{u\text{eff}}$) under tensile and compressive strains, despite $K_{u\text{eff}}$ also being slightly affected by the bending strains.

To have a better understanding of the physical mechanism of the bending-curvature-dependent magnetic properties, the magnetization-reversal kinetics of single-crystalline BaM films with different bending curvatures are simulated by micromagnetic simulations. We assume α is the angle between local magnetization, M, and the crystalline c axis, and β is the angle between M and the bending strain, ε_b. We have $\alpha + \beta = \pi/2$ for the case where the distribution of the crystalline c axis of the BaM film is ignored, as shown in Fig. 4(a). Then the magnetoelastic

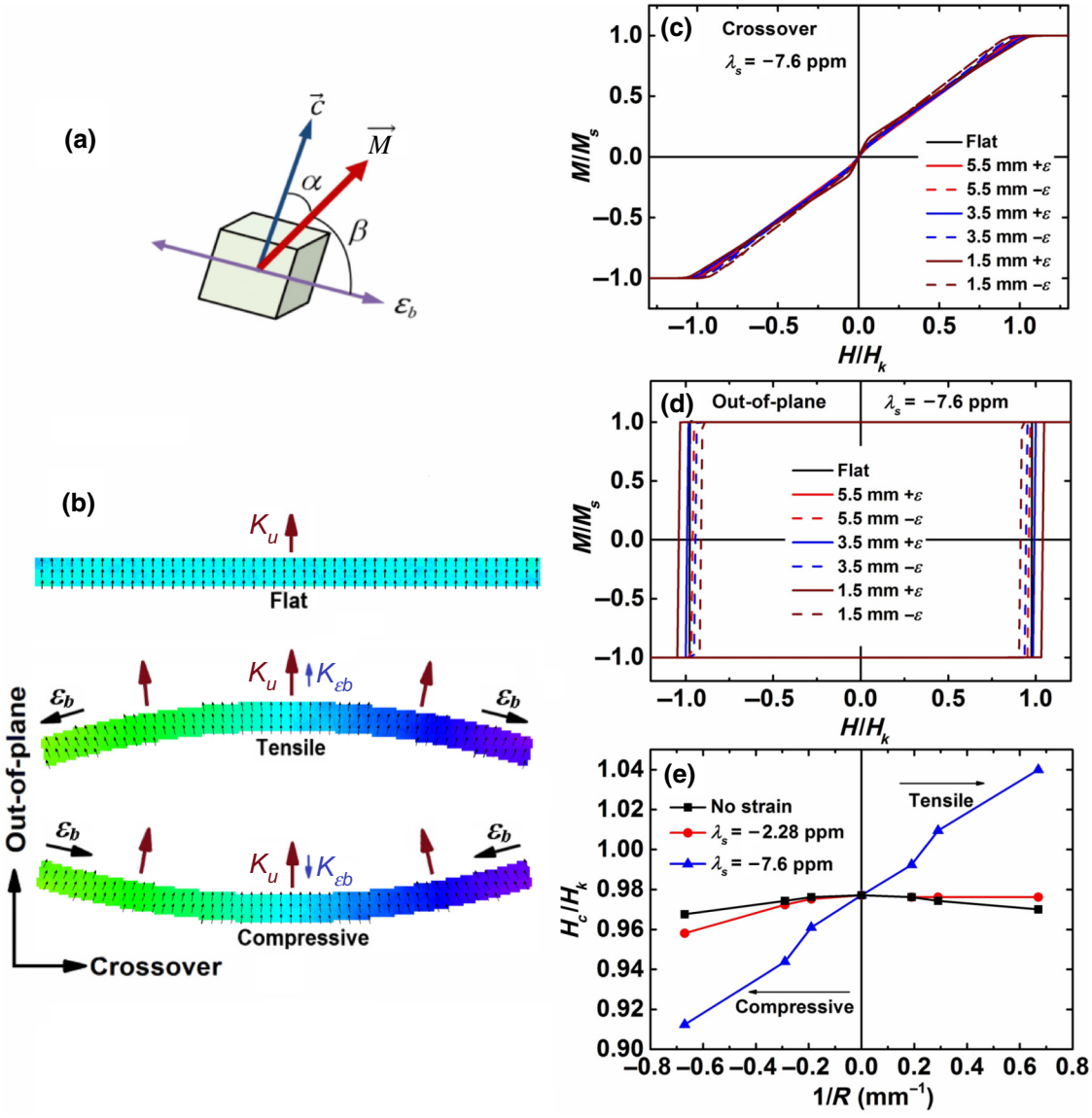

FIG. 4. (a) Schematic of a micromagnetic calculation cell with directions of local magnetization, M; crystalline c axis; and bending strain, ε_b, indicated. (b) Examples of simulated cross-section remanent magnetic domains of flat and bent BaM films; directions of K_u and K_{ε_b} are indicated. (c) Crossover and (d) out-of-plane hysteresis loops of films with different bending radii: $R = \infty$ (flat), 5.5, 3.5, and 1.5 mm. Tensile ($+\varepsilon$) and compressive ($-\varepsilon$) strains are indicated. (e) Bending-radius-dependent normalized out-of-plane coercivities, H_c/H_k, with different saturation magnetostriction constants ($\lambda_s = 0, \quad -2.28$, and -7.6 ppm).

anisotropy energy can be included in our micromagnetic model as

$$E_{\mathrm{el}} = -\frac{3}{2}\lambda_s E_f \varepsilon_b \cos^2\beta = K_{\varepsilon_b}\sin^2\alpha, \tag{5}$$

where λ_s ($\lambda_s = -7.6$ ppm for bulk BaM) [38] and E_f are the saturation magnetostriction constant and Young's modulus of BaM film, respectively. $K_{\varepsilon_b} = -(3/2)\lambda_s E_f \varepsilon_b$ is the stress-induced anisotropy constant, where $K_{\varepsilon_b} > 0$ under tensile strain ($\varepsilon_b > 0$) and $K_{\varepsilon_b} < 0$ under compressive strain ($\varepsilon_b < 0$). Therefore, the total anisotropy energy of the strained BaM film can be written as $E_{\mathrm{ani}} = (K_u + K_{\varepsilon_b})\sin^2\alpha$. With the M_s and K_u values taken from Fig. 2, the simulated magnetization-reversal process of BaM films with different bending radii are obtained, as shown in Fig. 4. Figure 4(b) shows that magnetization reversal takes places first from the ages of the bent film. This indicates that the magnetization-reversal process of the BaM film is affected by the bending geometry. Figures 4(c)–4(e) show that the hysteresis loops of the film change under different bending radii and strain directions. If $\lambda_s = 0$ (without strain), changes to the out-of-plane coercivities, H_c, are symmetrical under tensile and compressive strains. When $\lambda_s = -2.28$ ppm, slight asymmetry appears, so the tensile strain increases H_c and compressive strain decreases H_c. When λ_s is increased to -7.6 ppm, the changes to out-of-plane coercivities are asymmetrical under tensile and compressive strains. From a comparison between the simulation results and the experimental results, it can be concluded that the magnetization-reversal process of the BaM films is dominated by the film geometry (shape anisotropy) instead of stress anisotropy. The influence of

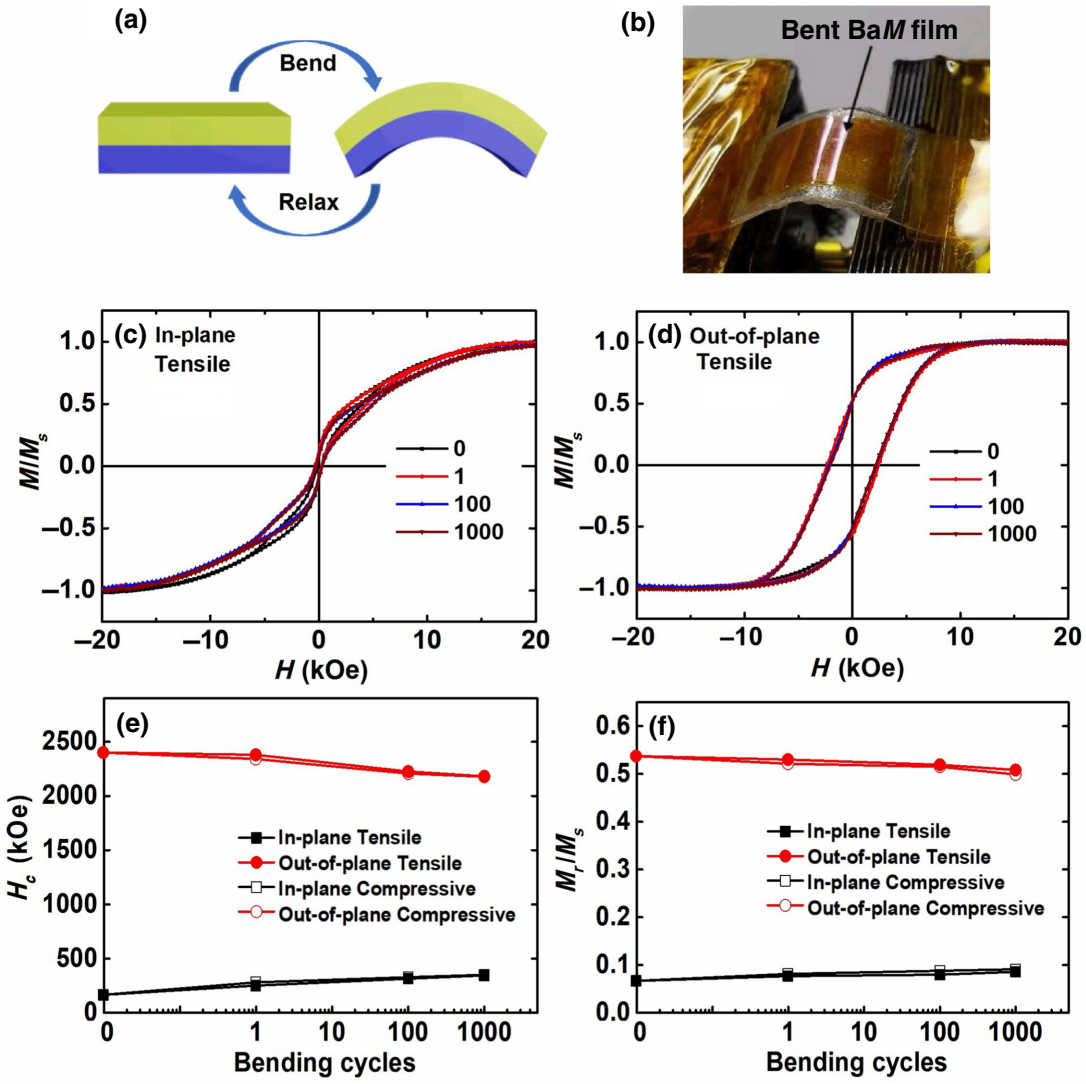

FIG. 5. (a) Schematic picture of a bending cycle of BaM film. (b) Picture of bent BaM film on the bending fixture. (c),d) In-plane and out-of-plane hysteresis loops of BaM film in different bending cycles (from 0 to 1000), with a tensile bending radius of 3.5 mm. (e),(f) Summaries of coercivity, H_c, and M_r/M_s in different bending cycles and under different bending conditions, respectively.

stress anisotropy on the magnetic properties of the Ba*M* film can be reduced by both its high K_u and low saturation magnetostriction constant [39,40].

C. Bending-cycle-dependent magnetic properties of Ba*M* thin films

The antifatigue property of flexible Ba*M* thin films is an important factor for device applications. To further understand the mechanical bending stability of the flexible Ba*M* film, the magnetic properties of the flexible Ba*M* film in different bending cycles are investigated.

Figure 5 provides the in-plane and out-of-plane hysteresis loops of the Ba*M* film in different bending cycles. Figures 5(c)–5(f) show that the hysteresis loops are very stable, with only very minor decreases of H_c (M_r/M_s) up to 1000 bending cycles. In addition, Figs. 5(e) and 5(f) show that there are no significant differences in the physical properties between tensile and compressive cycles. This indicates that a flexible Ba*M* film has excellent mechanical bending repeatability. Our SEM images show that the Ba*M* film is mechanically stable without breaking, but local minor defects can still exist after 1000 bending cycles [30]. These local bending defects can act as pinning centers for domain-wall motions in the film, and thus, change the magnetic properties of the film [19].

For a better understanding of the effects of bending defects on the magnetic bending stability of the Ba*M* film, the magnetic properties of curved thin films with different K_u and different types of cracks are studied by micromagnetic simulations. Figure 6(a) shows the simulated cross-section remanent domain images of two types of local cracks: a single crack of different sizes and multiple cracks with the same size. Figures 6(b)–6(d) show the magnetic field dependence of the total magnetic anisotropy energy, E_k, of the Ba*M* film. Local cracks in the film corresponds to an additional shape anisotropy in local positions, which add to the total magnetic anisotropy energy, E_k, and affect the magnetization-reversal process. The peak of E_k corresponds to the position of coercivity. Figure 6(b) shows that the peak of E_k varies greatly with the states of cracks in low-K_u films. The influence of local cracks on E_k is reduced sharply when K_u increases above 9×10^4 J/m^3. The high K_u corresponds to a high magnetocrystalline anisotropy energy, which suppresses local defect-induced shape anisotropy. Therefore, increasing K_u increases the

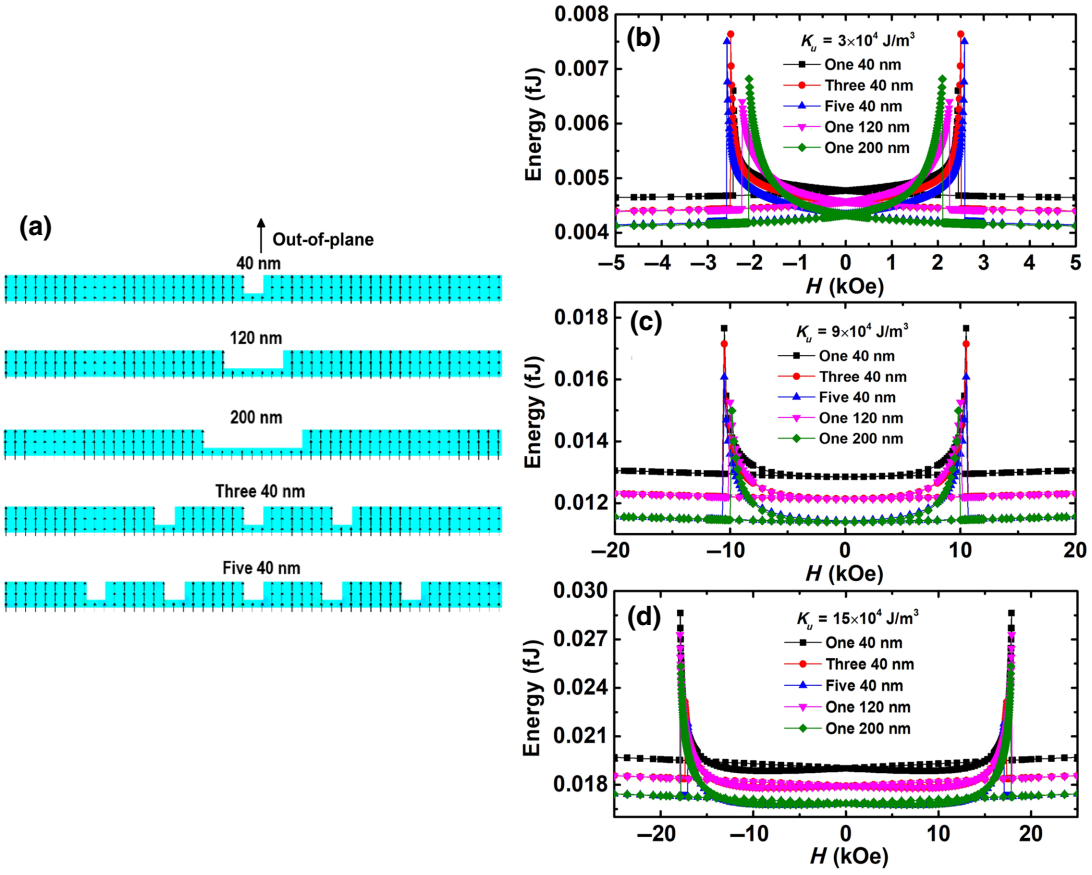

FIG. 6. (a) Simulated cross-section remanent domain images of Ba*M* films with different sizes (40, 120, and 200 nm) and numbers (one, three, and five) of cracks. Magnetic field dependence of total magnetic anisotropy energy, E_k, of Ba*M* films with (b) $K_u = 3 \times 10^4$ J/m^3, (c) $K_u = 9 \times 10^4$ J/m^3, and (d) $K_u = 15 \times 10^4$ J/m^3.

magnetic stability of the film. The good bending stability of the flexible BaM film should be partially attributed to its high K_u. The above results also suggest a method for the design of flexible magnetic thin films with better magnetic bending repeatability.

IV. CONCLUSION

In this work, hexaferrite BaM thin films are epitaxially grown on mica substrate and made flexible by substrate thinning. The flexible BaM thin film shows a room-temperature K_u of 1.1×10^5 J/m^3 and M_s of 151 emu/cm^3, corresponding to an anisotropy field, H_k, of 15.1 kOe. This high H_k supports out-of-plane zero-field ferromagnetic resonance above 35 GHz. The continuous and controllable tuning of magnetic parameters is found to be realizable with different bending radii of the film. Changes to the magnetic parameters are symmetrical under tensile and compressive bending due to the dominance of the film geometry and bending-stress directions, which are perpendicular to the easy axis of K_u. Micromagnetic simulations further show that the magnitude of K_u plays a critical role in the mechanical tuning performance of the film, where high K_u drastically reduces the role of stress anisotropy and increases the magnetic bending repeatability of the film by suppressing bending-defect-related anisotropy degradation. This work not only provides an understanding of the role of the direction and magnitude of K_u in flexible thin films, but also demonstrates that the flexible hexaferrite film is one of the best materials for mechanically tunable devices up to the millimeter-wave region.

ACKNOWLEDGMENTS

This work is financially supported by the National Natural Science Foundation of China (Grant No. 51772200).

[1] D. Weller, A. Moser, L. Folks, M. E. Best, W. Lee, M. F. Toney, M. Schwickert, J. U. Thiele, and M. F. Doerner, High K_u materials approach to 100 Gbits/in^2, IEEE Trans. Magn. **36**, 10 (2000).

[2] J. M. D. Coey, Hard magnetic materials: A perspective, IEEE Trans. Magn. **47**, 4671 (2011).

[3] L. Liu, Q. Qin, W. N. Lin, C. J. Li, Q. D. Xie, S. H. He, X. Y. Shu, C. H. Zhou, Z. S. Lim, J. H. Yu, W. L. Lu, M. S. Li, X. B. Yan, S. J. Pennycook, and J. S. Chen, Current-induced magnetization switching in all-oxide heterostructures, Nat. Nanotechnol. **14**, 939 (2019).

[4] V. G. Harris, A. Geiler, Y. J. Chen, S. D. Yoon, M. Z. Wu, A. Yang, Z. H. Chen, P. He, P. V. Parimi, X. Zuo, C. E. Patton, M. Abe, O. Acher, and C. Vittoria, Recent advances in processing and applications of microwave ferrites, J. Magn. Magn. Mater. **321**, 2035 (2009); V. G. Harris and A. S. Sokolov, The self-biased circulator: ferrite materials design and process considerations, J. Supercond. Nov. Magn. **32**, 97 (2019).

[5] J. Inoue, H. Onoda, and H. Yanagihara, Uniaxial magnetic anisotropy of transition metal oxides: Role of local lattice deformation, J. Phys. D: Appl. Phys. **53**, 195003 (2020).

[6] Z. Z. Cui, A. J. Grutter, H. Zhou, H. Cao, Y. Q. Dong, D. A. Gilbert, J. Y. Wang, Y. S. Liu, J. J. Ma, Z. P. Hu, J. H. Guo, J. Xia, B. J. Kirby, P. Shafer, E. Arenholz, H. H. Chen, X. F. Zhai, and Y. L. Lu, Correlation-driven eightfold magnetic anisotropy in a two-dimensional oxide monolayer, Sci. Adv. **6**, eaay0114 (2020).

[7] E. K. Ko, J. Mun, H. G. Lee, J. Kim, J. Song, S. H. Chang, T. H. Kim, S. B. Chung, M. Kim, L. Wang, and T. W. Noh, Oxygen vacancy engineering for highly tunable ferromagnetic properties: A case of $SrRuO_3$ ultrathin film with a $SrTiO_3$ capping layer, Adv. Funct. Mater. **30**, 2001486 (2020).

[8] M. Melzer, J. I. Mönch, D. Makarov, Y. Zabila, G. S. C. Bermúdez, D. Karnaushenko, S. Baunack, F. Bahr, C. Yan, M. Kaltenbrunner, and O. G. Schmidt, Wearable magnetic field sensors for flexible electronics, Adv. Mater. **27**, 1274 (2015).

[9] D. Makarov, M. Melzer, D. Karnaushenko, and O. G. Schmidt, Shapeable magnetoelectronics, Appl. Phys. Rev. **3**, 011101 (2016).

[10] P. Sheng, B. M. Wang, and R. W. Li, Flexible magnetic thin films and devices, J. Semicond. **39**, 1 (2018).

[11] M. Liu, B. M. Howe, L. Grazulis, K. Mahalingam, T. Nan, N. X. Sun, and G. J. Brown, Voltage-impulse-induced non-volatile ferroelastic switching of ferromagnetic resonance for reconfigurable magnetoelectric microwave devices, Adv. Mater. **25**, 4886 (2013).

[12] L. Chen, F. Matsukura, and H. Ohno, Direct-current voltages in (Ga, Mn)As structures induced by ferromagnetic resonance, Nat. Commun. **4**, 2055 (2013).

[13] T. Nozaki, Y. Shiota, S. Miwa, S. Murakami, F. Bonell, S. Ishibashi, H. Kubota, K. Yakushiji, T. Saruya, A. Fukushima, S. Yuasa, T. Shinjo, and Y. Suzuki, Electric-field-induced ferromagnetic resonance excitation in an ultrathin ferromagnetic metal layer, Nat. Phys. **8**, 491 (2012).

[14] N. Spaldin and M. Fiebig, The renaissance of magnetoelectric multiferroics, Science **309**, 391 (2005).

[15] J. Lou, M. Liu, D. Reed, Y. Ren, and N. X. Sun, Giant electric field tuning of magnetism in novel multiferroic FeGaB/lead zinc niobate–lead titanate (PZN-PT) heterostructures, Adv. Mater. **21**, 4711 (2009).

[16] P. C. Wu, P. F. Chen, T. H. Do, Y. H. Hsieh, C. H. Ma, T. D. Ha, K. H. Wu, Y. J. Wang, H. B. Li, Y. C. Chen, J. Y. Juang, P. Yu, L. M. Eng, C. F. Chang, P. W. Chiu, L. H. Tjeng, and Y. H. Chu, Heteroepitaxy of Fe_3O_4/muscovite: A new perspective for flexible spintronics, ACS. Appl. Mater. Interfaces. **8**, 33794 (2016).

[17] Y. H. Chu, Van der Waals oxide heteroepitaxy, npj Quantum Mater. **2**, 67 (2017); T. Amrillah, Y. Bitla, K. Shin, T. Yang, Y. H. Hsieh, Y. Y. Chiou, H. J. Liu, T. H. Do, D. Su, Y. C. Chen, S. U. Jen, L. Q. Chen, K. H. Kim, J. Y. Juang, and Y. H. Chu, Flexible multiferroic bulk heterojunction with giant magnetoelectric coupling via van der waals epitaxy, ACS Nano. **11**, 6122 (2017); H. Liu, C. Wang, D. Su, T. Amrillah, Y. Hsieh, K. Wu, Y. Chen, J. Juang, L. M. Eng, S. Jen, and Y. H. Chu, Flexible heteroepitaxy of

$CoFe_2O_4$/muscovite bimorph with large magnetostriction, ACS Appl. Mater. Interfaces **9**, 7297 (2017).

[18] F. An, K. Qu, G. K. Zhong, Y. Q. Dong, W. J. Ming, M. F. Zi, Z. J. Liu, Y. D. Wang, B. Y. Qi, Z. Ding, J. Xu, Z. L. Luo, X. S. Gao, S. H. Xie, P. Gao, and J. Y. Li, Highly flexible and twistable freestanding single crystalline magnetite film with robust magnetism, Adv. Funct. Mater. **30**, 2003495 (2020).

[19] L. Shen, L. Wu, Q. Sheng, C. Ma, Y. Zhang, L. Lu, J. Ma, J. Ma, J. Bian, Y. Yang, A. Chen, X. Lu, M. Liu, H. Wang, and C.-L. Jia, Epitaxial lift-off of centimeter-scaled spinel ferrite oxide thin films for flexible electronics, Adv. Mater. **29**, 1702411 (2017).

[20] Y. Zhang, L. Shen, M. Liu, X. Li, X. Lu, L. Lu, C. Ma, C. You, A. Chen, C. Huang, L. Chen, M. Alexe, and C. L. Jia, Flexible quasi-two-dimensional $CoFe_2O_4$ epitaxial thin films for continuous strain tuning of magnetic properties, ACS Nano **11**, 8002 (2017).

[21] W. L. Liu, M. Liu, R. Ma, R. Y. Zhang, W. Q. Zhang, D. P. Yu, Q. Wang, J. N. Wang, and H. Wang, Epitaxial lift-off of centimeter-scaled spinel ferrite oxide thin films for flexible electronics, Adv. Mater. **29**, 1702411 (2017).

[22] Y. N. Zhao, Y. J. Li, Z. Y. Zhou, R. C. Peng, S. K. Zhu, M. T. Yao, B. Peng, Y. F. Zhao, Y. X. Cheng, B. Tian, Z. Q. Hu, Z. G. Ye, Z. D. Jiang, and M. Liu, Low-damping flexible $Y_3Fe_5O_{12}$ thin films for tunable RF/microwave processors, Mater. Horiz. **7**, 1558 (2020).

[23] R. C. Pullar, Hexagonal ferrites: A review of the synthesis, properties and applications of hexaferrite ceramics, Prog. Mater. Sci. **57**, 1191 (2012).

[24] M. Sugimoto, The past, present, and future of ferrites, J. Am. Ceram. Soc. **82**, 269 (1999).

[25] T. Suzuki, T. Tanaka, and K. Ikemizu, High density recording capability for advanced particulate media, J. Magn. Magn. Mater. **235**, 159 (2001).

[26] Z. H. Chen, A. Yang, A. Gieler, V. G. Harris, C. Vittoria, P. R. Ohodnicki, K. Y. Goh, M. McHenry, Z. H. Cai, T. L. Goodrich, and K. S. Ziemer, Epitaxial growth of *M*-type Ba-hexaferrite films on MgO(111)‖SiC(0001) with low ferromagnetic resonance linewidths, Appl. Phys. Lett. **91**, 182505 (2007).

[27] B. L. Hu, Z. J. Su, S. Bennett, Y. J. Chen, and V. G. Harris, High quality Y-type hexaferrite thick films for microwave applications by an economical and environmentally benign crystal growth technique, J. Appl. Phys. **115**, 17A513 (2014).

[28] I. Harward, Y. Nie, D. M. Chen, J. Baptist, J. M. Shaw, E. J. Liskova, S. Visnovsky, P. Siroky, M. Lesnak, J. Pistora, and Z. Celinski, Physical properties of Al doped Ba hexagonal ferrite thin films, J. Appl. Phys. **113**, 043903 (2013).

[29] V. K. Lazarov, P. J. Hasnip, Z. Cai, K. Yoshida, and K. S. Ziemer, Dynamically stabilized growth of polar oxides: The case of MgO(111), J. Appl. Phys. **109**, 07E520 (2011).

[30] See the Supplemental Material at http://link.aps.org/supplemental/10.1103/PhysRevApplied.16.054006 for a schematic of the sample fabrication process, bending-dependent surface microstructures (SEM images), and thickness-dependent magnetic properties (magnetic force microscopy and hysteresis loops) of flexible Ba*M* thin films.

[31] M. J. Donahue, and D. G. Porter, Pengantar Belajar Object Oriented Micromagnetic Framework (OOMMF) 1.2a4, http://math.nist.gov/oommf/

[32] P. Novák and J. Rusz, Exchange interactions in barium hexaferrite, Phys. Rev. B **71**, 184433 (2005).

[33] T. Ono, N. Kikuchi, S. Okamoto, O. Kitakami, and T. Shimatsu, Novel torque magnetometry for uniaxial anisotropy constants of thin films and its application to FePt granular thin films, Appl. Phys. Express. **11**, 033002 (2018).

[34] P. Cavallotti, R. Roberti, A. Cartoceti, and F. Scansetti, Mechanical properties of barium hexaferrites, IEEE. Trans. Magn. **MAG-15**, 3 (1979).

[35] G. Dong, *et al.*, Super-elastic ferroelectric single-crystal membrane with continuous electric dipole rotation, Science **366**, 475 (2019); Y. N. Zhao, R. C. Peng, Y. T. Guo, Z. J. Liu, Y. Q. Dong, S. S. Zhao, Y. J. Li, G. H. Dong, Y. Hu, J. W. Zhang, Y. Peng, T. N. Yang, B. Tian, Y. F. Zhao, Z. Y. Zhou, Z. D. Jiang, Z. L. Luo, and M. Liu, Multiferroic heterostructures: ultraflexible and malleable $Fe/BaTiO_3$ multiferroic heterostructures for functional devices, Adv. Funct. Mater., 2009376 (2021).

[36] K. Gu, T. Katayama, S. Yasui, A. Chikamatsu, S. Yasuhara, M. Itoh, and T. Hasegawa, Simple method to obtain large-size single-crystalline oxide sheets, Adv. Funct. Mater. **30**, 2001236 (2020).

[37] F. Eskandari, S. B. Porter, M. Venkatesan, P. Kameli, K. Rode, and J. M. D. Coey, Magnetization and anisotropy of cobalt ferrite thin films, Phys. Rev. Mater. **1**, 074413 (2017).

[38] A. G. Chesnokov and E. P. Naiden, Influence of diamagnetic cations Sc^{3+} on the magnetoelastic energy of M-type hexaferrites, Phys. Solid. State **43**, 1728 (2001).

[39] Q. C. Sun, S. N. Baker, A. D. Christianson, and J. L. Musfeldt, Magnetoelastic coupling in bulk and nanoscale MnO, Phys. Rev.B. **84**, 014301 (2011).

[40] U. Oezguer, Y. Alivov, and H. Morkoc, Microwave ferrites, part 1: Fundamental properties, J. Mater. Sci: Mater Electron **20**, 789 (2009).